

A COMPARISON OF HINDCAST AND MEASURED WAVE SPECTRA

Graham Feld
Fugro GEOS, Inc.
6100 Hillcroft,
Houston, Texas, USA

Gunnar Mørk
Fugro OCEANOR AS
Pir-Senteret
N-7462 Trondheim, Norway

1. INTRODUCTION

Assessment of the operability of floating structures can depend considerably upon the wave conditions that impact a particular site. Definition of spectral shapes are also significant for response-based design techniques. To these ends, parameterised directional wave spectra are often used as input to vessel response algorithms. The source of these wave spectra can be either measured or, more often, hindcast wave spectra. The aim of the study that is described in this paper is to assess the consistency of spectral shapes amongst hindcast and measured data sets. To achieve this comparison, contemporaneous and co-locational deepwater directional wave spectra were analysed from one location in the Gulf of Mexico and from one in the West of Shetlands region.

In order to fit to individual wind-sea and swell components of the spectra, they were partitioned using an approach similar to that described in Hanson and Phillips (2001). Each component was then fitted to a JONSWAP spectrum via a least-squares fitting procedure. A quantitative comparison was then carried out on the JONSWAP parameters via quantile-quantile plots produced for H_s-T_p pairs across a scatter diagram for each location, and via comparison of their medians.

2. DATA SETS

The data sets that were used for the analysis are indicated in Table 1.

	Gulf of Mexico	West of Shetland
Measured data		
Source	NDBC buoy 42001	Seawatch buoy
Location	25.84 N 89.66 W	60.31N, 4.33W
Model data		
Source	ECMWF	AES40
Location	26.00 N, 89.50 W	60.00 N, 5.00 W
Period	Jan – Dec 2002	Jan – Jul 1995

Table 1 Data sets used in the analysis

The Gulf of Mexico data sources were within 15nm of each other, while the West of Shetland locations were around 45nm apart.

More detail regarding each of these data sets and the methods by which directional spectra were synthesised are given in the following sections.

2.1 Gulf of Mexico Measured Data

The Gulf of Mexico measured data that were used came from NDBC buoy 42001, which is situated in the mid-Gulf 180nm south of Southwest Pass, Louisiana. The buoy is a 12-meter discus type deployed in a water depth of 3,246m. Data from the year 2002 were obtained and this period included the effects of Hurricanes Isidore and Lili. The data comprised of 20-minute samples taken every hour with spectral information available at a range of frequencies from 0.02Hz to 0.485Hz. In the range of significant energy, the bandwidths were 0.005Hz below 0.1Hz and 0.01Hz above it.

At each frequency, f , the following parameters were available:

S	spectral energy density in m^2/Hz
D	mean wave direction, in degrees from true North
r_1	$[(a_1^2 + b_1^2)^{0.5}]/a_0$
r_2	$[(a_2^2 + b_2^2)^{0.5}]/a_0$
α_1	$270 - \tan^{-1}(b_1/a_1)$
α_2	$270 - (0.5 * \tan^{-1}(b_2/a_2) + \{0 \text{ or } 180\})$

where a_1 , b_1 , a_2 and b_2 are the first and second Fourier coefficients as described in Longuet-Higgins *et al* (1963). In order to avoid negative energy densities at some frequency-direction combinations a weighted average version of the Fourier sum was used, i.e.:

$$S(f, \theta) = \frac{1}{\pi} \left(0.5 + \frac{2}{3} r_1 \cos(\theta - \alpha_1) + \frac{1}{6} r_2 \cos(2(\theta - \alpha_2)) \right)$$

The effect of this was to widen the apparent directional spread of the energy peaks. The purpose, however, of this stage of data preparation was to produce a directional spectrum that would assist in the identification, and subsequent partitioning, of separate wind-sea and swell components. The details of the directional spread itself were not of critical importance to this study. The

directional resolution that was used for the reconstruction of the spectra was 15° .

In order to make the data more comparable with the wave spectra from the model data, the spectra were averaged over 6 hours. In all, this produced 1,429 spectra with the directional and frequency resolutions described above.

2.2 Gulf of Mexico Model Data

The model data that were used for the comparison was taken from the European Centre for Medium Range Weather Forecasts operational WAM model. Spectra from this model are available globally on a 0.5° grid with a time step of 6 hours. The data that were used for this study had a directional resolution of 15° and had a frequency range from 0.03452Hz to 0.54764Hz with 30 frequency bands. The frequencies that are available from the model are geometrically rather than linearly spaced, which aids in the calculation of interactions between energy at different frequencies. The resolution of the frequency spectrum, though, was of the same order as that from the measured data.

A comparison of the ECMWF H_s measurements against those measured by NDBC buoy 42001 over the period 05 December 1996 to 10 August 2002 is given in Figure 1.

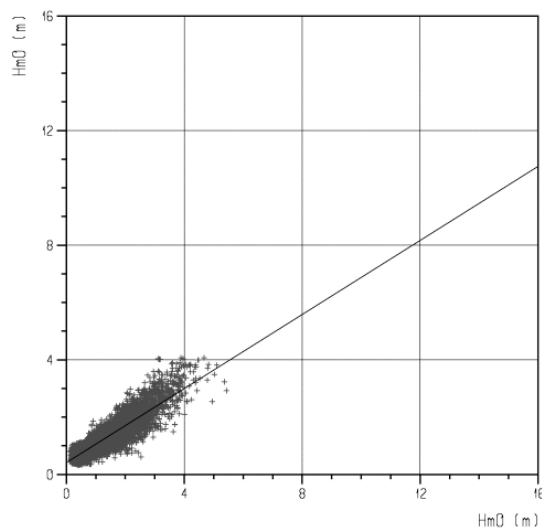


Figure 1 ECMWF (y-axis) v NDBC 42001 (x-axis) H_s

Although the regression line indicates that the model data under-predicted the wave heights as compared with the buoy, this was largely due to differences at very low wave heights that skewed the regression line. The plot indicates that there is a good agreement between the two data sets for H_s values from around 1m upwards. A detailed calibration of ECMWF wave heights and periods is currently on-going for the whole of the Gulf of Mexico (and worldwide) by Fugro OCEANOR AS as part of the development of WorldWaves, and this will be completed by the end of 2004.

The ECMWF wave data were used “as is” for the purpose of this paper.

2.3 West of Shetland Measured Data

The measured spectra from the West of Shetland were donated by BP for the purposes of this study. The data were measured using a Seawatch directional wave rider buoy in approximately 500m of water with samples taken every 30 minutes. The stored output from this sensor consisted of energy, direction and spreading parameters at 64 frequencies ranging from 0.025Hz to 0.58Hz. For frequencies less than 0.1Hz, the bandwidth was 0.005Hz, above that frequency it was 0.01Hz.

At each frequency, the following parameters were available:

- S spectral energy density in m^2/Hz
- a_1, b_1 first Fourier coefficients
- a_2, b_2 second Fourier coefficients

These parameters were used to derive full 2-dimensional directional frequency spectra using the maximum entropy method (Lygre and Krogstad, 1986). The data were averaged over 6 hours, as for the NDBC data, but they were also smoothed due to the somewhat spiky nature of the resultant spectra, using a 9-point block averaging scheme. The “sides” and “corners” were averaged across reduced blocks of 6 and 4, respectively, reflecting the fact that complete blocks of 9 were truncated for these direction-frequency combinations.

Due to periods of missing data, only 443 spectra were produced by this analysis from the 7-month period.

2.4 West of Shetland Model Data

Oceanweather, Inc. donated AES40 data to the study for comparison with the measured data in the West of Shetland region. The hindcast model is based on 3rd generation physics on a 0.625 by 0.833 degree grid. The closest available spectra were from grid point 7207 at $60.0N, 5.00W$.

The resolution of the data was 15° in direction and there were 23 frequency bins ranging from 0.039Hz to 0.3216Hz. As for the ECMWF data, these bins were geometrically spaced and gave similar frequency resolution to the other data sets. No additional calibration was applied to the data before its use in this study.

3. COMPARISON OF TOTAL SEA STATE PARAMETERS

As a gross check on the agreement between the measured and model data from each of the two locations, time series plots and quantile-quantile plots were made of the overall time series of H_s and T_p . The plots are shown in Figure 2 to Figure 4 for the Gulf of Mexico and in Figure 5 to Figure 7 for the West of Shetland. The Gulf of Mexico plots show good agreement between the H_s values, but

with a slight underestimation at and around storm peaks. During the summer months, it is evident that the model slightly over-predicts the very low energy sea states and it is this feature which is largely responsible for the skewed regression shown in Figure 1. This is probably due to too much trade wind swell energy entering from the Caribbean – this feature has as of 2003 been corrected by ECMWF). The two large events at the end of September and the beginning of October are Hurricanes Isidore and Lili, respectively and these storms are in fact reasonably well modelled by this operational model.

The peak wave periods show considerably more scatter between the measured and model data. The latter tends to

overestimate the wave periods during the low energy summer season for the reason given above (swells entering from the Caribbean). Overall, the agreement between the two data sets, however, was considered sufficiently good to allow a meaningful comparison of the spectral shapes on a scatter diagram basis.

For the West of Shetland measured data, there are more gaps than for the Gulf of Mexico data, as indicated in the time series plots of Figure 5 and Figure 6. However, the agreement between the data sets where there are data is good and again provides a sound basis for spectral shape comparison.

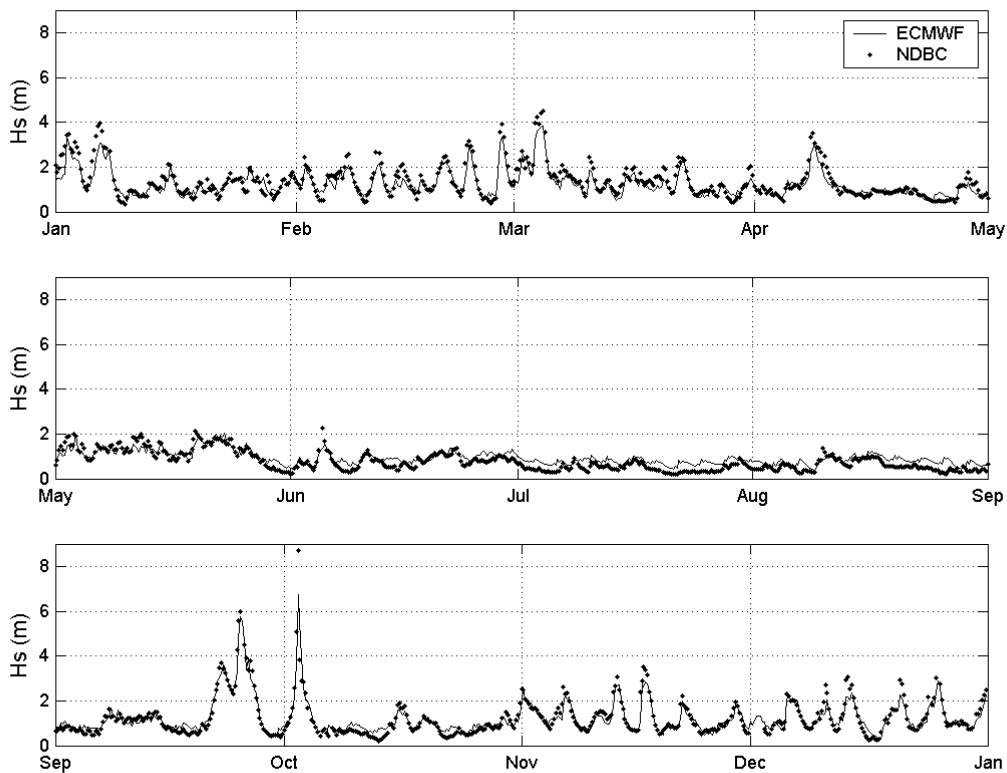


Figure 2 Time series of H_s from ECMWF and NDBC buoy 42001 for the year 2002

4. SPECTRAL ANALYSIS AND PARTITIONING

Each of the directional spectra data sources that are described in Section 2 were partitioned to split the spectra into individual wind-sea and swell components. This was achieved via the use of a partitioning algorithm based on work by Gerling (1992), Hasselmann *et al* (1994) and more latterly by Hanson and Phillips (2001) and Aarnes and Krogstad (2001). The latter two papers presented an

approach by which directional wave spectra could be partitioned by the use of a steepest ascent matrix approach. This allows a domain of attraction to be determined for each frequency-direction pair. This 2-dimensional approach to partitioning spectra allows considerably more detail to be resolved than simply by looking at the omni-directional spectrum.

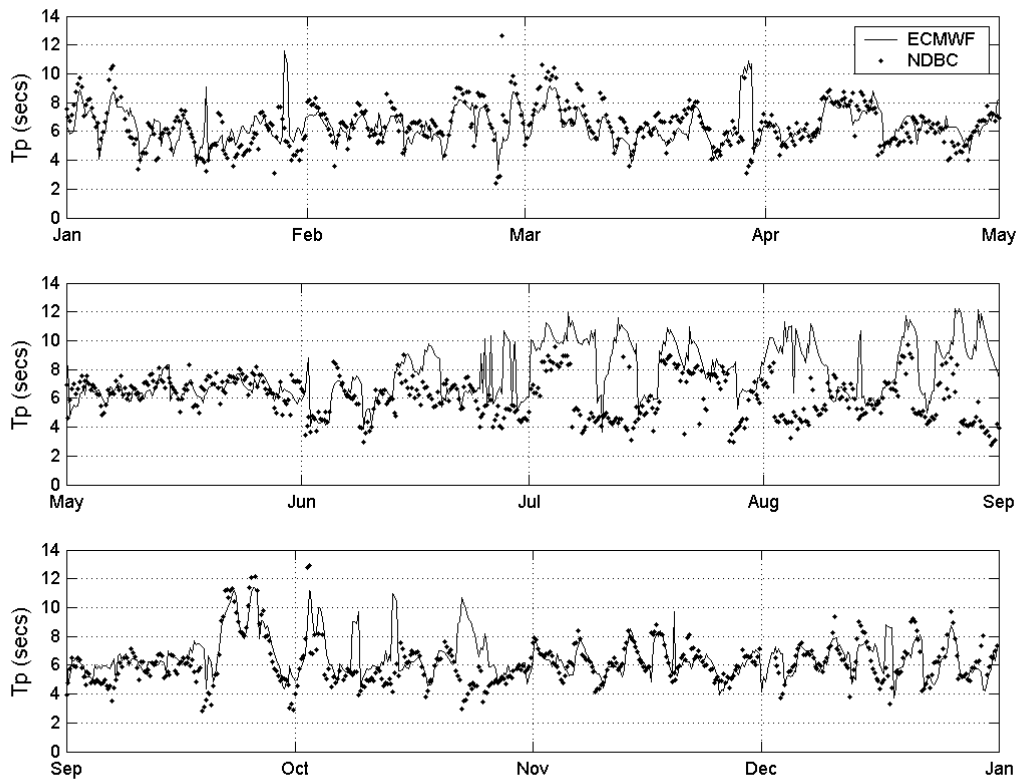


Figure 3 Time series of T_p from ECMWF and NDBC buoy 42001 for the year 2002

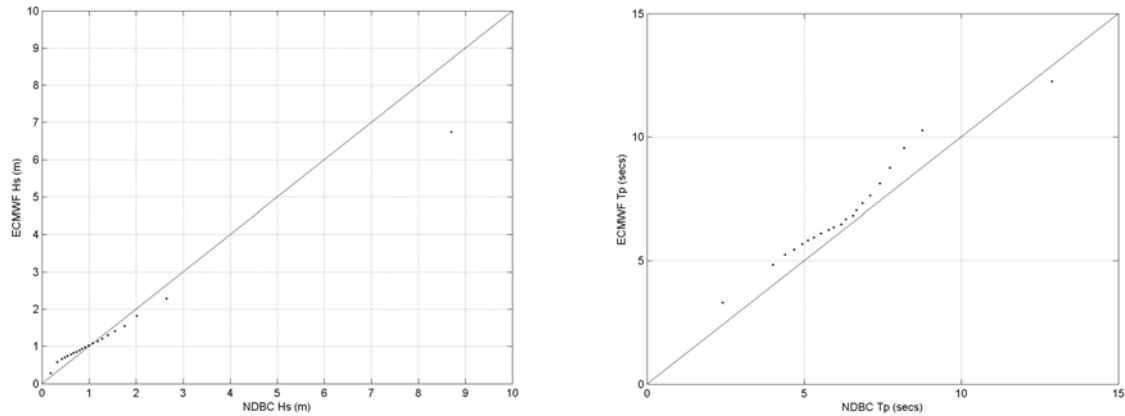


Figure 4 Quantile-quantile plots of H_s and T_p from ECMWF and NDBC buoy 42001 for the year 2002

Inevitably with measured data, noise and natural sampling variability can produce spurious spectral peaks that need to be identified. To try to optimise the correct identification of real versus apparent spectral peaks, Hanson and Phillips (2001) and Aarnes and Krogstad (2001) describe the following steps and diagnostic checks:

- all peaks that have a propagation direction within 90° of the wind and have a phase speed less than a certain

factor, ρ , times the wind speed are combined into a single wind-sea partition;

- two swell partitions are combined if the Euclidean distance between adjacent peaks is less than a factor, κ , times the spread of the peaks; or, if the saddle point value between two peaks is greater than a certain factor, ν , times the lower of two adjacent peaks.

- partitions with energy less than a certain threshold value are combined with adjacent partitions, i.e. partitions are combined if:

$$E_p < \frac{a}{f_m^4 + b}$$

where, E_p is the partition energy, f_m is the partition peak frequency and a and b are parameters that can be tuned to the data set in question. Table 2 presents the values that were used for the two measured data sets.

	Gulf of Mexico	West of Shetland
ρ	1.33	1.33
κ	0.4	0.05
ν	0.85	0.96
a	5.10^{-5}	9.10^{-6}
b	1.10^{-2}	3.10^{-2}

Table 2 Values of partitioning parameters

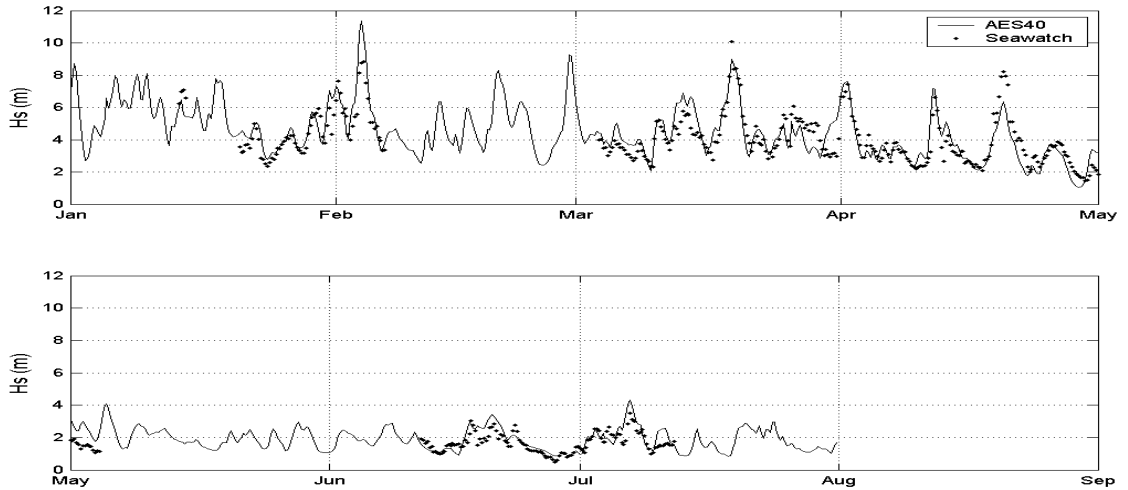


Figure 5 Time series of H_s from AES40 and the Seawatch buoy for Jan-Jul 1995

With model data, the problem is more of identifying spectral peaks that may be “hidden” in the data, since there is no noise or sampling variability. This typically occurs when a secondary peak produces a “shoulder” in the primary spectrum. The partitioning algorithm that was used for this paper could not identify the secondary partition under these circumstances.

5. SPECTRAL PARAMETERISATION

A JONSWAP spectrum was fitted to each identified partition. The following steps were followed to achieve this:

- The energy in each partition was summed to produce an omni-directional frequency distribution.
- To identify the peak frequency, f_m , a parabola was fitted to the highest spectral density estimate and one point either side as in the Gunther method, described in Tucker and Pitt (2001).
- Again, as in the Gunther method, Phillips’ constant α was calculated by assuming that the spectrum in the range $1.35f_m$ to $2.00f_m$ could be approximated by a P-M spectrum.

- The remaining JONSWAP parameters, γ , σ_a and σ_b were then calculated by using a least squares fit to the omni-directional spectrum. If γ was calculated to be less than 1, then a P-M spectrum was assumed. In these circumstances, f_m and α were fitted by a least squares approach.
- As in Tucker and Pitt (2001), a normalised rms error and a bias were calculated to assess the goodness of fit. These parameters were used as a means of selecting reliable spectral fits for the quantitative comparison between measured and model data.
- The direction at the peak frequency was derived by first deriving the directional energy distribution at the peak frequency, f_m . A parabola was then fitted to the peak direction and one point on either side to determine the peak direction.

6. COMPARISON OF SPECTRAL PARAMETERS

This section presents the results from the fitting of the spectral parameters to each of the data sets. Only those spectral partitions that were fitted with an absolute bias of $<5\%$ and with an rms error of less than 0.05 were used in the comparison given below.

Each identified spectral partition was placed into its appropriate Hs - Tp bin of size 1 metre by 2 seconds. The derived values of γ , α , σ_a and σ_b were aggregated in each bin and their medians calculated. The median values rather than the mean values were chosen as representative of each

bin in order to eliminate the effect of very large values (particularly in the case of γ) skewing the comparative statistics. Scatter diagrams of the medians are shown in plots in the top half of the pages at the end of the paper.

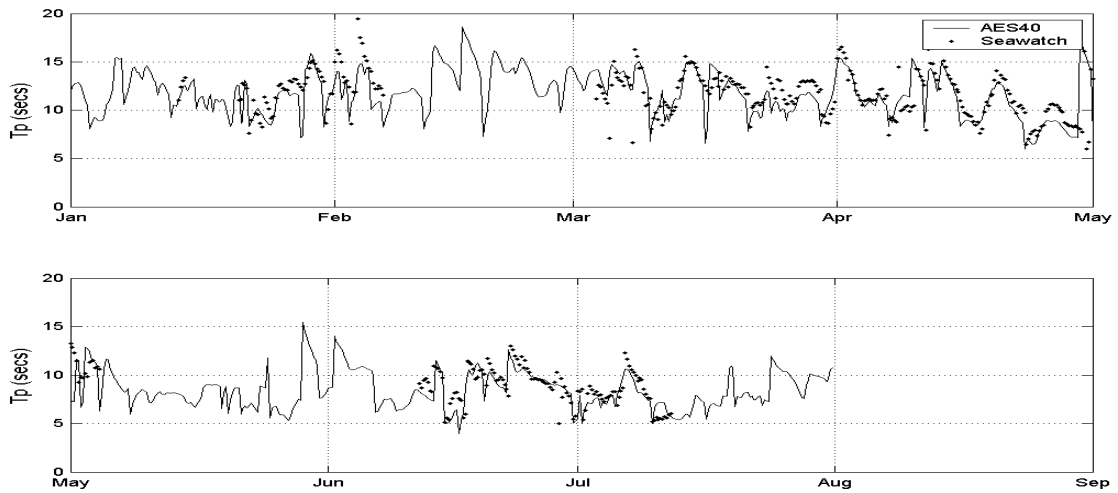


Figure 6 Time series of Tp from AES40 and the Seawatch buoy for Jan-Jul 1995

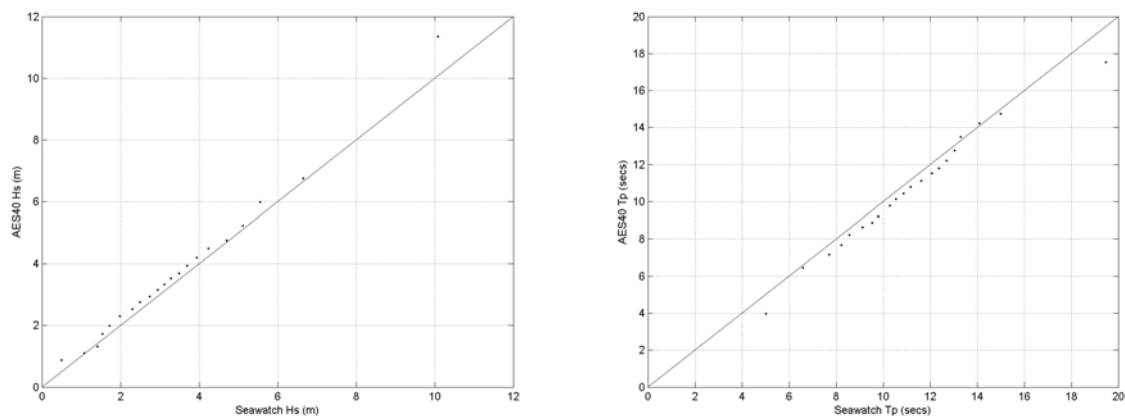


Figure 7 Quantile-quantile plots of Hs and Tp from AES40 and the Seawatch buoy for common periods during Jan-Jul 1995

For those Hs - Tp bins where there were at least 5 occurrences available from both the measured and model data sets, a quantile-quantile plot was produced to allow a more general comparison of the parameter values. In the plots in the bottom halves of the pages at the end of the paper, the dots represent quantiles from 10 to 90; the diagonals are the $y=x$ line; and, the values given above each represent the mid Hs - Tp values for each bin. The results for Hs values in the 0.0-1.0m range (i.e. those bins notated as Hs 0.5m) should be treated with somewhat more caution, due to the fact that noise plays more of a role in these spectra and consequently the fitting procedure is less reliable. The descriptions and conclusions therefore focus on sea states above this level.

6.1 Gulf of Mexico

The Gulf of Mexico plots are shown in Figure 8 to Figure 19. The median γ values are provided in the first two of these figures for the ECMWF and NDBC data sets. The steepest sea states from the former tend to have γ values around 1.8 – 2.1, which drop to around 1.6 - 1.8 as the steepness decreases. As we move further towards the bottom-right of the scatter diagram, towards the long-period swell (LPS) region, the γ values increase considerably and are much less consistent. These larger values are not surprising since swell often has a very small or even non-existent Phillips' tail, which makes any empirically-fitted γ value prone to very large variability.

The NDBC data have γ values for the steepest sea states in the range 2.5 – 5.1, once again decreasing with decreasing sea-state steepness, this time to around 2.2 – 2.5. The LPS region of the scatter diagram also follows the same pattern with much larger and scattered γ values. Figure 10 indicates that the NDBC data (shown on the y -axis of each plot) produce higher estimates of γ in nearly all cases where data are available from both data sources. Conversely, the α values from the NDBC data (shown on the y -axis of each plot) are generally lower than those from the ECMWF data. The implication from the two sets of plots is that the ECMWF spectra are somewhat broader-banded than those from the measured data.

The ECMWF σ_a values are generally higher than the NDBC data for the Gulf of Mexico (shown in Figure 14 to Figure 16). This reinforces the conclusion from the γ and α , plots that the model data peaks are broader than those in the measured data. The σ_b values in the next three figures are not so clear cut, with the median values being broadly similar between the two data sets. In the LPS region of the spectrum, the σ values are a better guide to peakedness than γ or α since they correspond directly to the width of the spectral peak and are much less prone to large variability. Here, once again, the model spectra are indicated as having broader spectra (i.e. larger σ values).

6.2 West of Shetland

The West of Shetland data are shown in Figure 20 to Figure 31. The γ values shown in the first three of these figures are once again higher for the measured data than for the model data, although this is less marked than for the Gulf of Mexico. The steepest sea states have median γ values in the range 1.5 – 2.0, decreasing to 1.0 – 1.3 before increasing into the LPS region. The measured Seawatch data decrease from around 1.8 – 3.0 to 1.2 – 1.5 before moving into the region of high variability in the bottom right of the figures.

Similar relationships are again evident for α as for the Gulf of Mexico, but with generally better agreement in the case of the West of Shetland data. The σ_a and σ_b plots imply that the AES40 model data generally produce slightly higher values than the measured data but not by much. There is particularly good agreement in the mid H_s - T_p range of the scatter diagram. Overall, the figures indicate that the AES40 spectra have slightly lower, narrower peaks than the measured data in most parts of the scatter diagram but have lower, broader peaks for LPS.

7. CONCLUSIONS

The results imply that hindcast model spectra are less peaked than those indicated by measured data. Therefore, if hindcast spectra were used as input to design and operability studies, this work implies that the peakedness may be underestimated. This has implications for

assessment of vessel operability, particularly if the frequencies of response are in the vicinity of spectral peaks.

The AES40 spectra did agree somewhat more closely with the measured data than did the ECMWF spectra in this study, there being closer agreement with the fitted JONSWAP parameters. At this stage, though, the comparison is anecdotal, being carried out only on specific data sets in specific regions and it is too early to say if the pattern revealed here is indicative of a generic trend. Additionally, the specific steps that have been carried out to produce these results are not definitive. For example: there is some doubt as to whether hindcast spectra should indeed be considered representative of 6 hours of data; and the “correct” degree of smoothing that is applied to measured spectra is hard to define. It is certainly the case, though, that if the measured spectra were to be averaged over less than 6 hours as comparison with the model data, the measured spectra are likely to be even more peaked, so providing a greater discrepancy between the measured and model data sets.

ACKNOWLEDGEMENTS

Great thanks are due to Oceanweather, Inc. for the donation of AES40 model data, and to BP for the West of Shetlands measured data for this study.

REFERENCES

- Aarnes, J.E. and Krogstad, H.E., 2001: Partitioning sequences for the dissection of directional ocean wave spectra: A review. Part of work package 4 (Wp4) of the EnviWave (EVG-2001-00017) research programme under the EU Energy, Environment and Sustainable Development programme.
- Gerling, T.W., 1992: Partitioning sequences and arrays of directional wave spectra into component wave systems. *J. Atmos. And Oceanic Technol.*, 9, 444-458.
- Hanson, J.L. and Phillips, O.M. 2001: Automated analysis of ocean surface directional wave spectra. *J. Atmos. Oceanic Technol.*, 18, 277-293.
- Hasselmann, S., Hasselmann, K., Bruning, C., 1994: Extraction of wave spectra from SAR image spectra. *Dynamics and Modelling of Ocean Waves*, G. Komen (ed.), Cambridge University Press, Cambridge, England, 391-401.
- Longuet-Higgins, M.S., Cartwright, D.E., Smith, N.D., 1963: Observations of the directional spectrum of sea waves using the motions of a floating buoy, *Ocean Wave Spectra*, Prentice-Hall, New Jersey, 111-136.
- Lygre, A., Krogstad, H.A., 1986: Maximum entropy estimation of the directional distribution in ocean wave spectra, *J. Phys. Ocean.*, Vol. 16, 12, 2052-2060
- Tucker, M.J. and Pitt, E.G., 2001: *Waves in ocean engineering*, R. Bhattacharyya & M.E. McCormick (eds.), Elsevier Ocean Engineering Book Series, Vol. 5, London

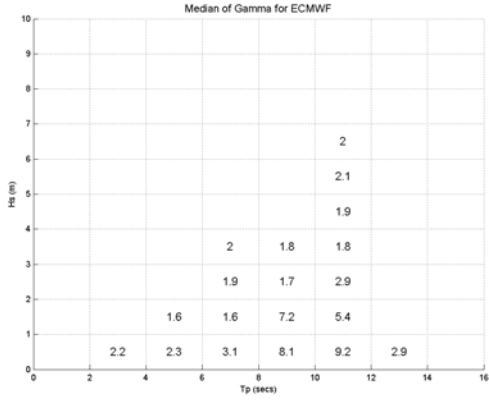


Figure 8 Median Gulf of Mexico ECMWF γ values

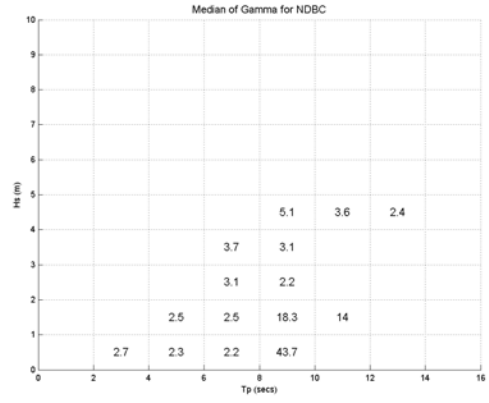


Figure 9 Median Gulf of Mexico NDBC γ values

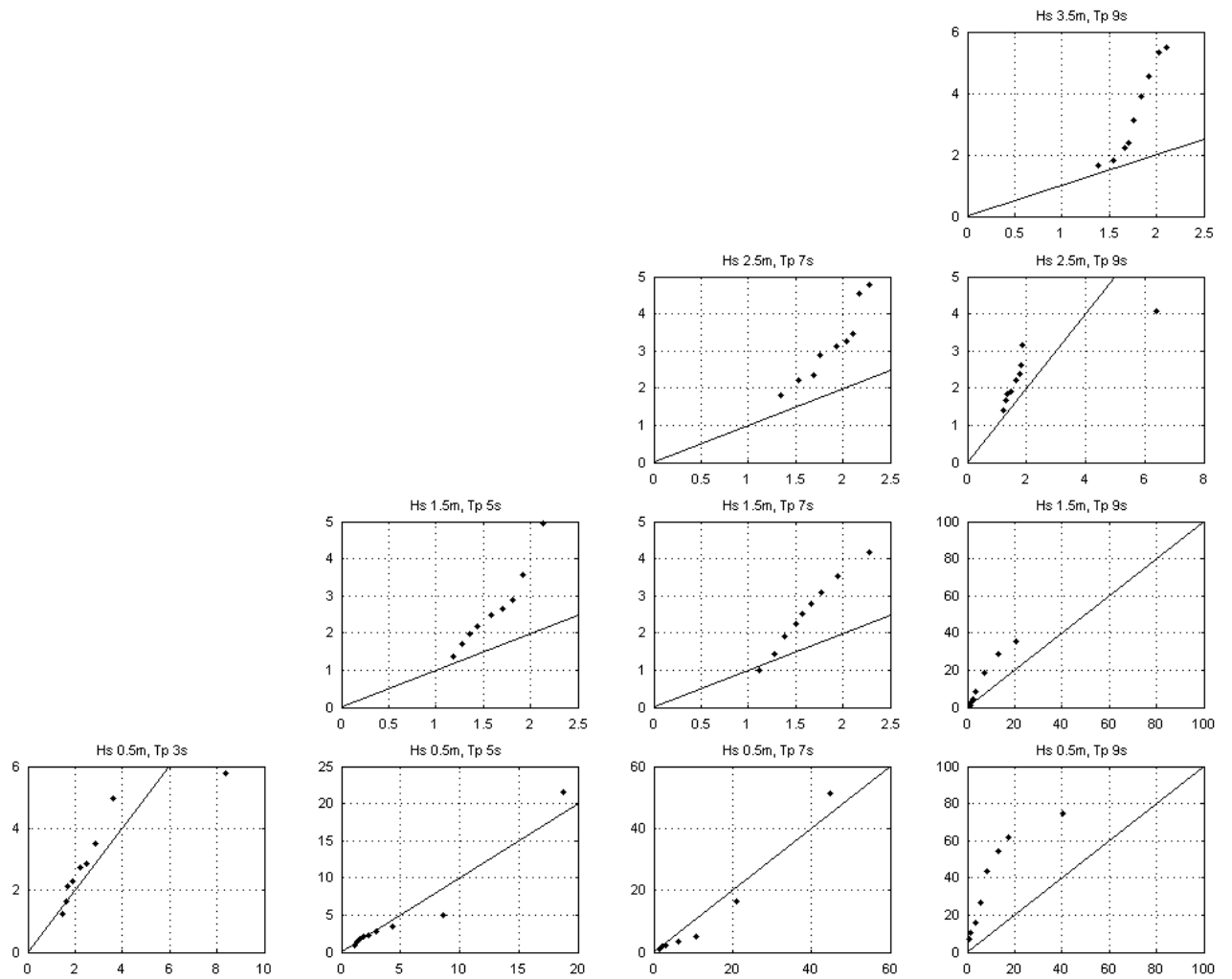


Figure 10 QQ plots for Gulf of Mexico γ data (y-axis NDBC, x-axis ECMWF)

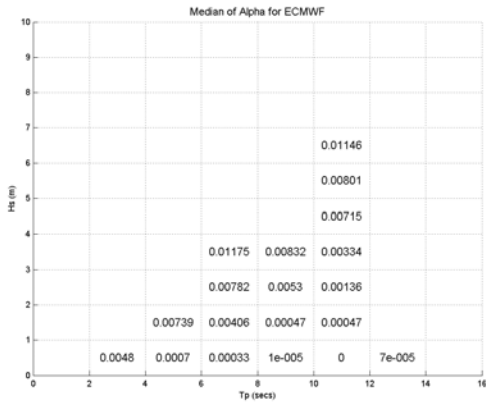


Figure 11 Median Gulf of Mexico ECMWF α values

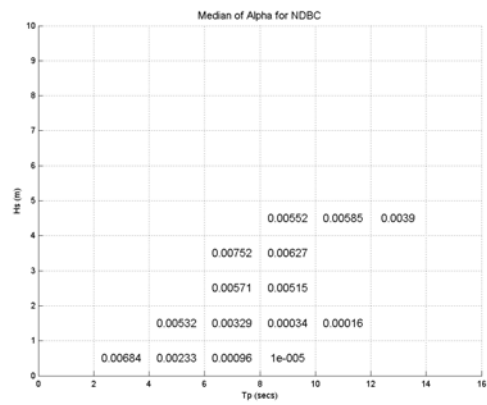


Figure 12 Median Gulf of Mexico NDBC α values

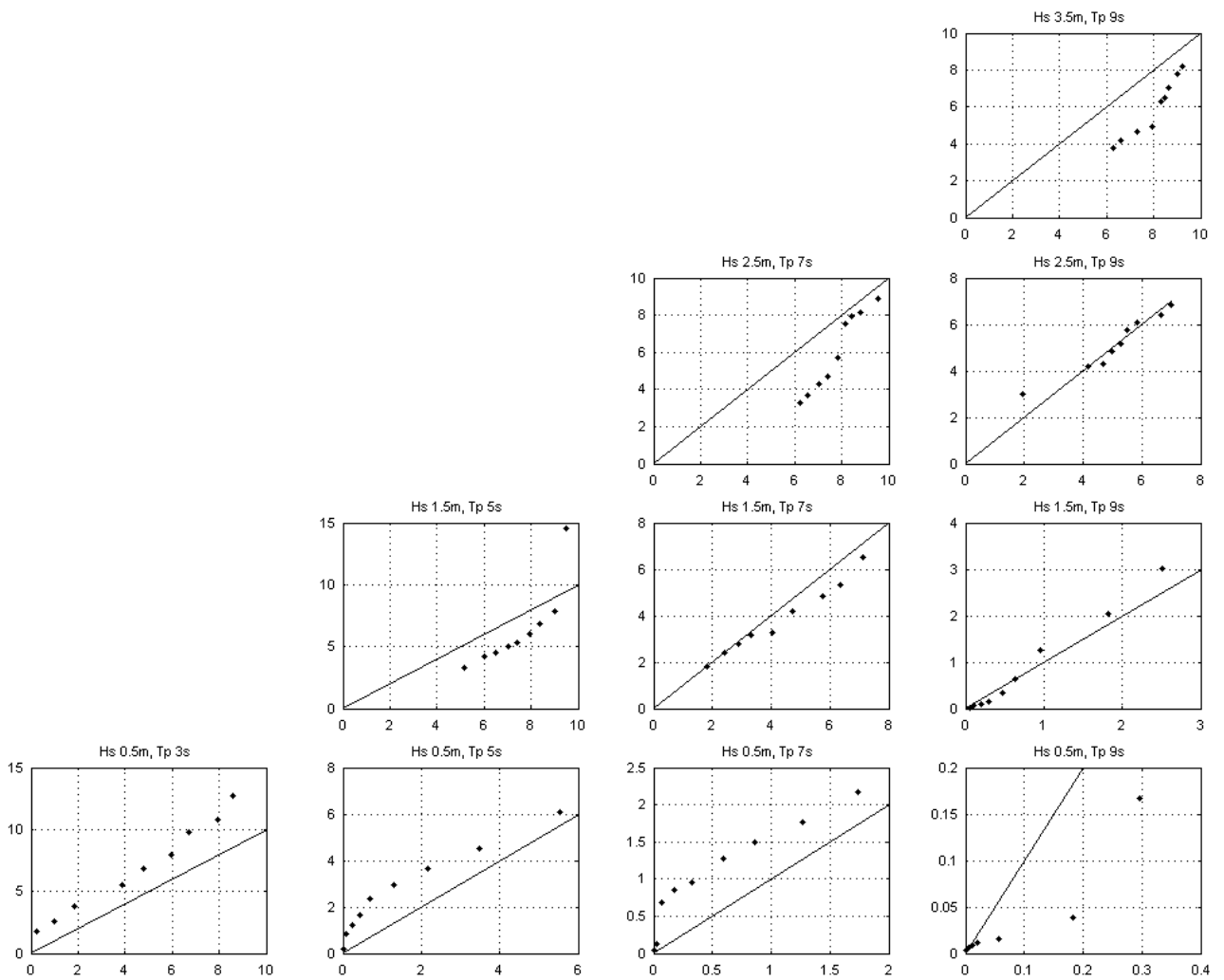


Figure 13 QQ plots for Gulf of Mexico $\alpha \cdot 10^3$ data (y-axis NDBC, x-axis ECMWF)

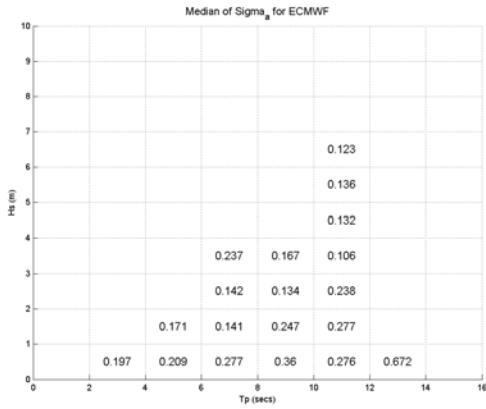


Figure 14 Median Gulf of Mexico ECMWF σ_a values

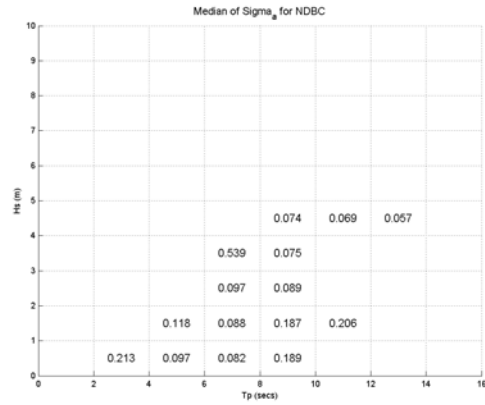


Figure 15 Median Gulf of Mexico NDBC σ_a values

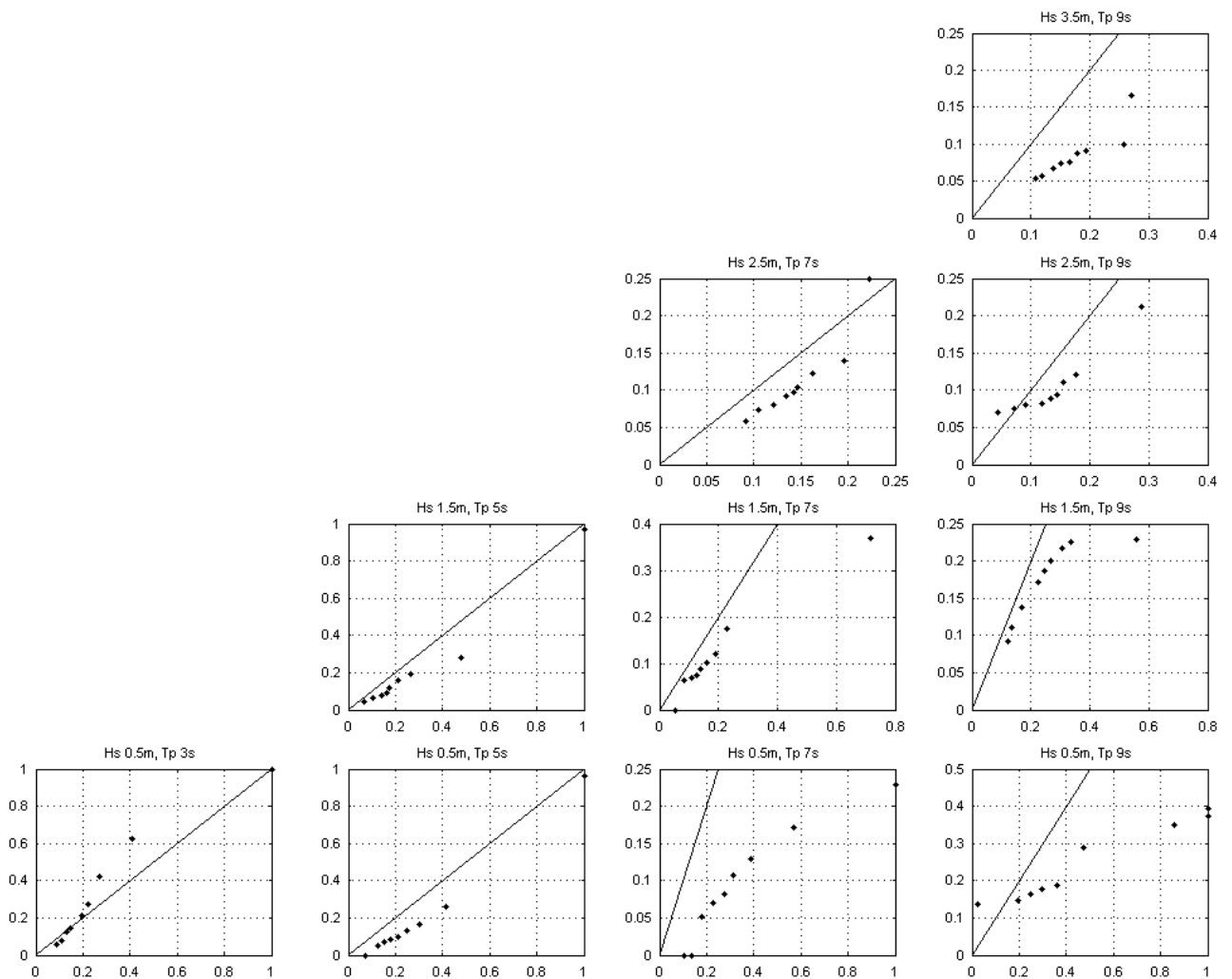


Figure 16 QQ plots for Gulf of Mexico σ_a data (y-axis NDBC, x-axis ECMWF)

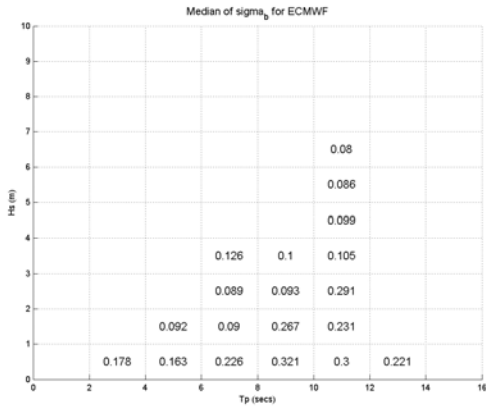


Figure 17 Median Gulf of Mexico ECMWF σ_b values

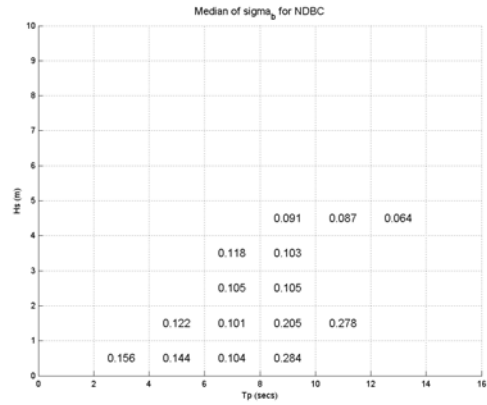


Figure 18 Median Gulf of Mexico NDBC σ_b values

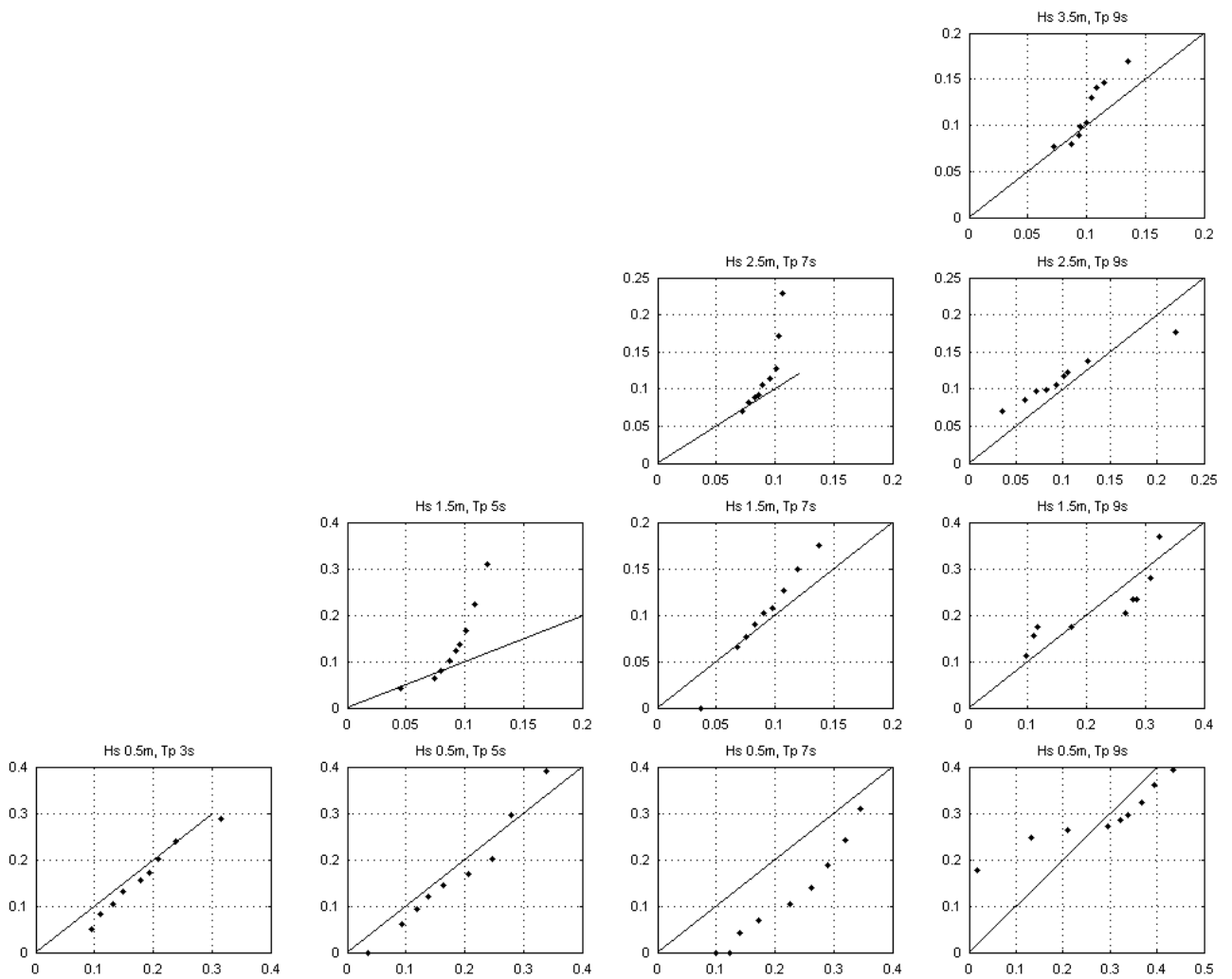


Figure 19 QQ plots for Gulf of Mexico σ_b data (y-axis NDBC, x-axis ECMWF)

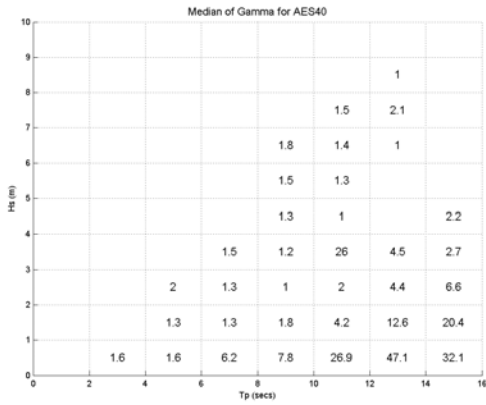


Figure 20 Median West of Shetland AES40 γ values

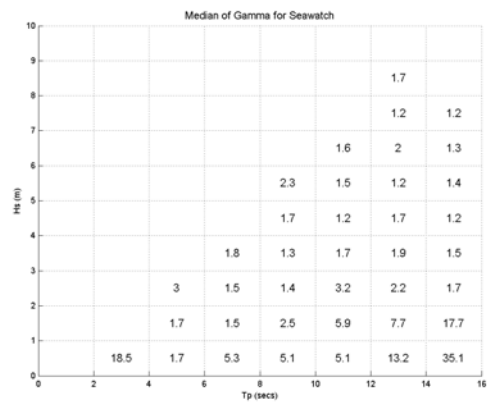


Figure 21 Median West of Shetland Seawatch γ values

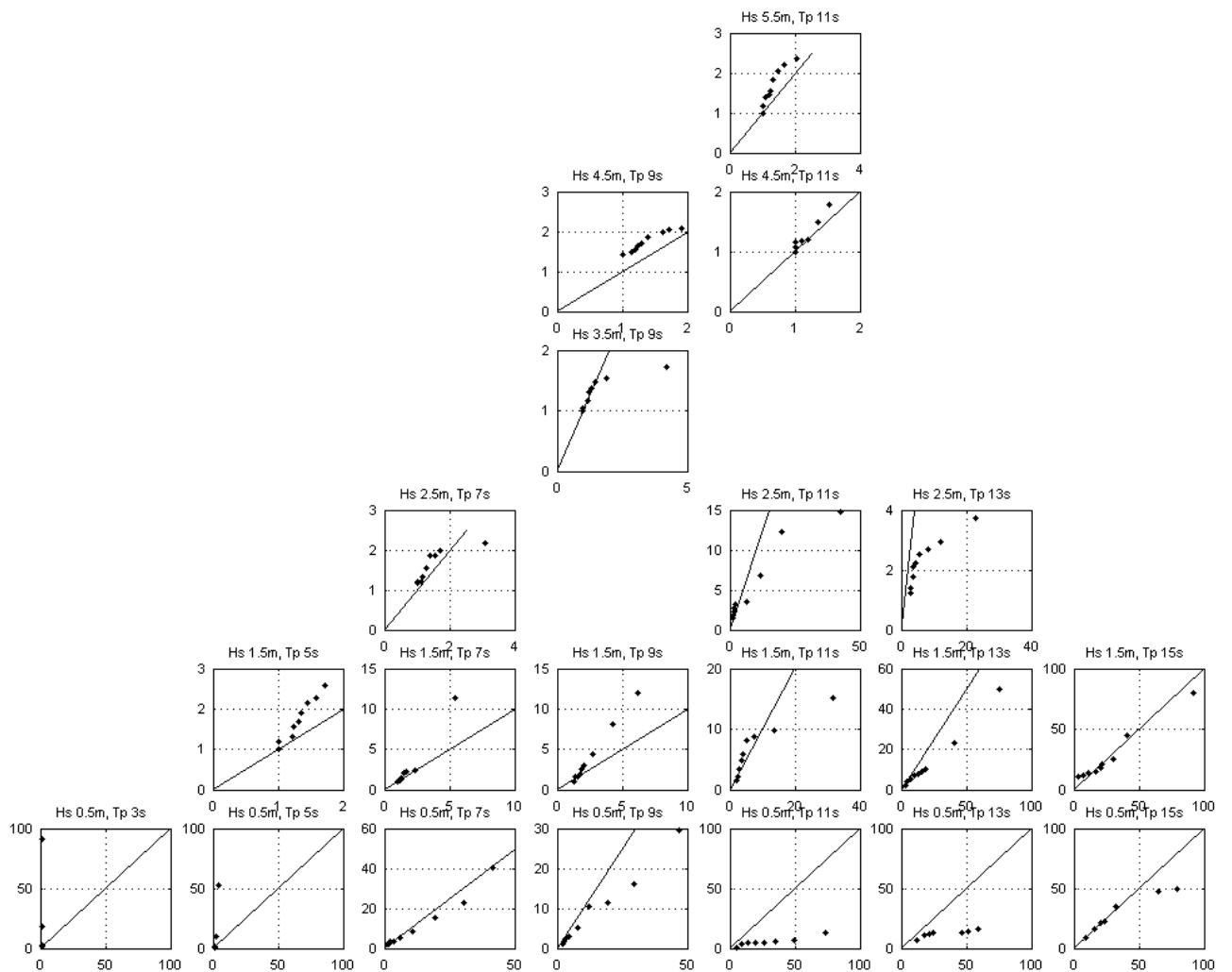


Figure 22 QQ plots for West of Shetland γ data (y-axis Seawatch, x-axis AES40)

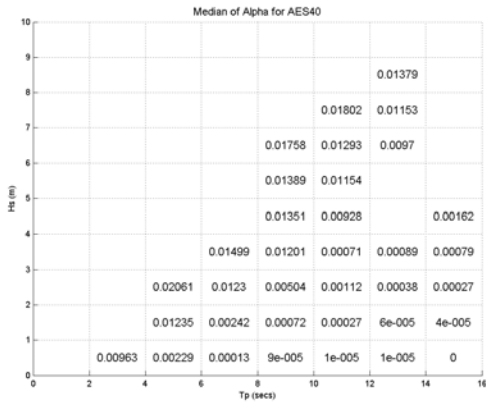


Figure 23 Median West of Shetland AES40 α values

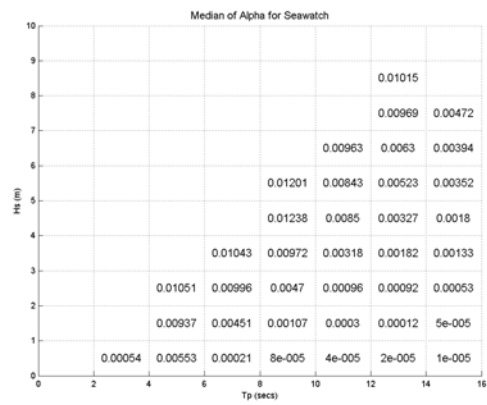


Figure 24 Median West of Shetland Seawatch α values

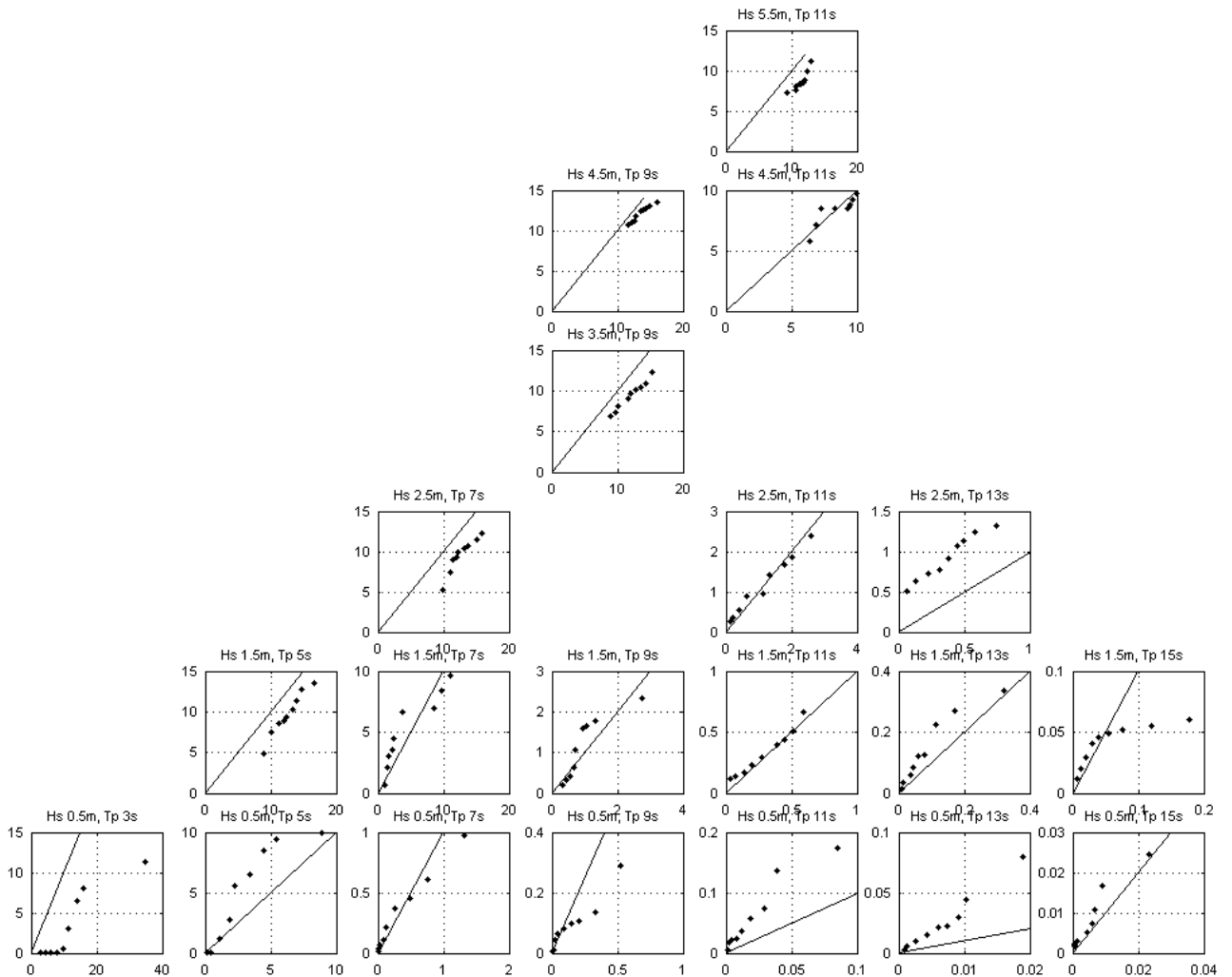


Figure 25 QQ plots for West of Shetland $\alpha \cdot 10^3$ data (y-axis Seawatch, x-axis AES40)

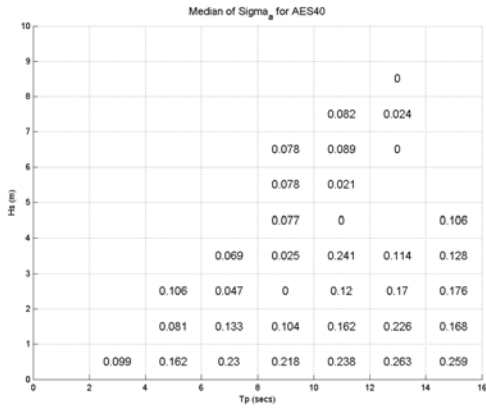


Figure 26 Median West of Shetland AES40 σ_a values

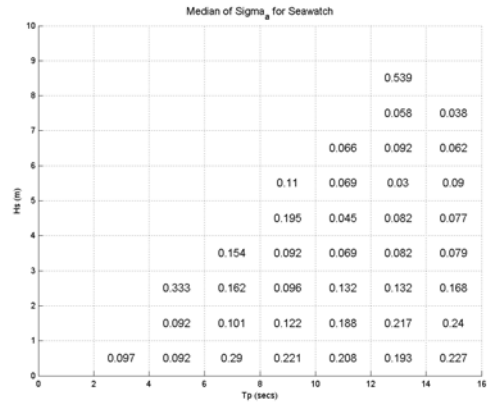


Figure 27 Median West of Shetland Seawatch σ_a values

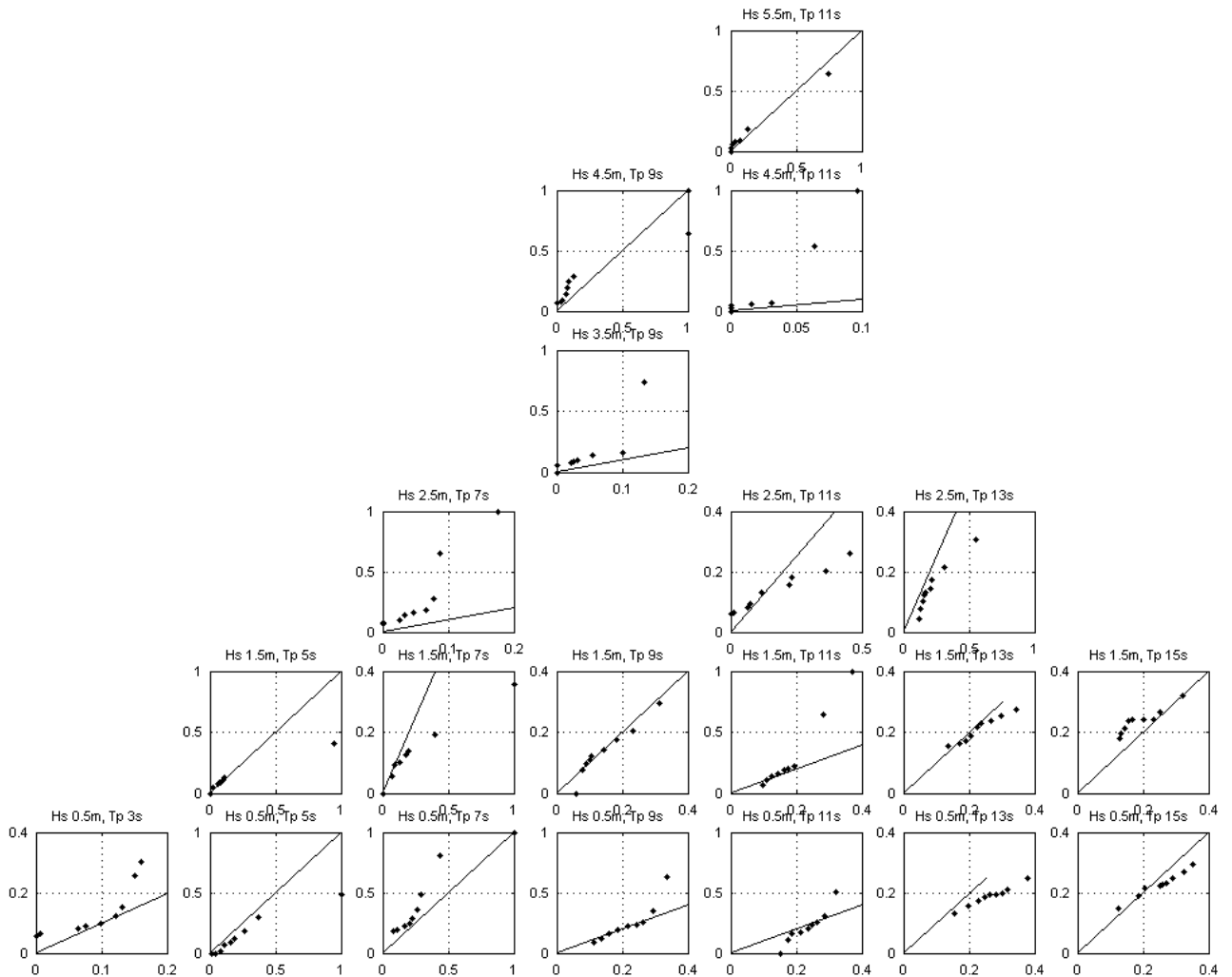


Figure 28 QQ plots for West of Shetland σ_a data (y-axis Seawatch, x-axis AES40)

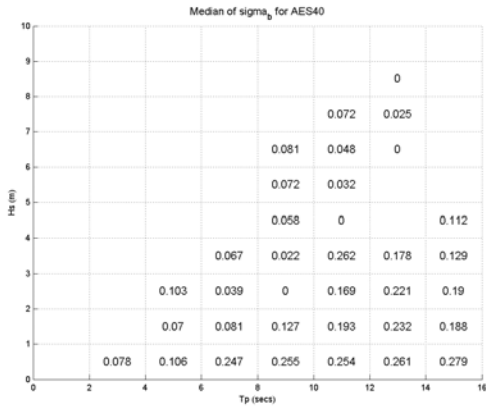


Figure 29 Median West of Shetland AES40 σ_b values

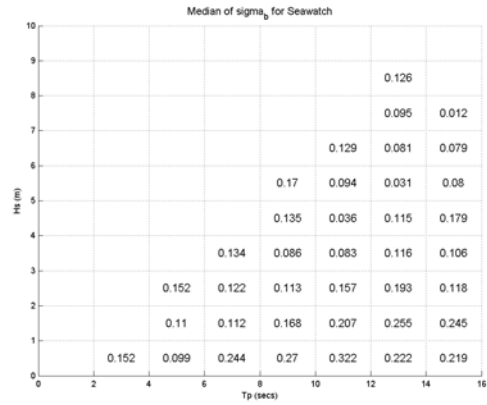


Figure 30 Median West of Shetland Seawatch σ_b values

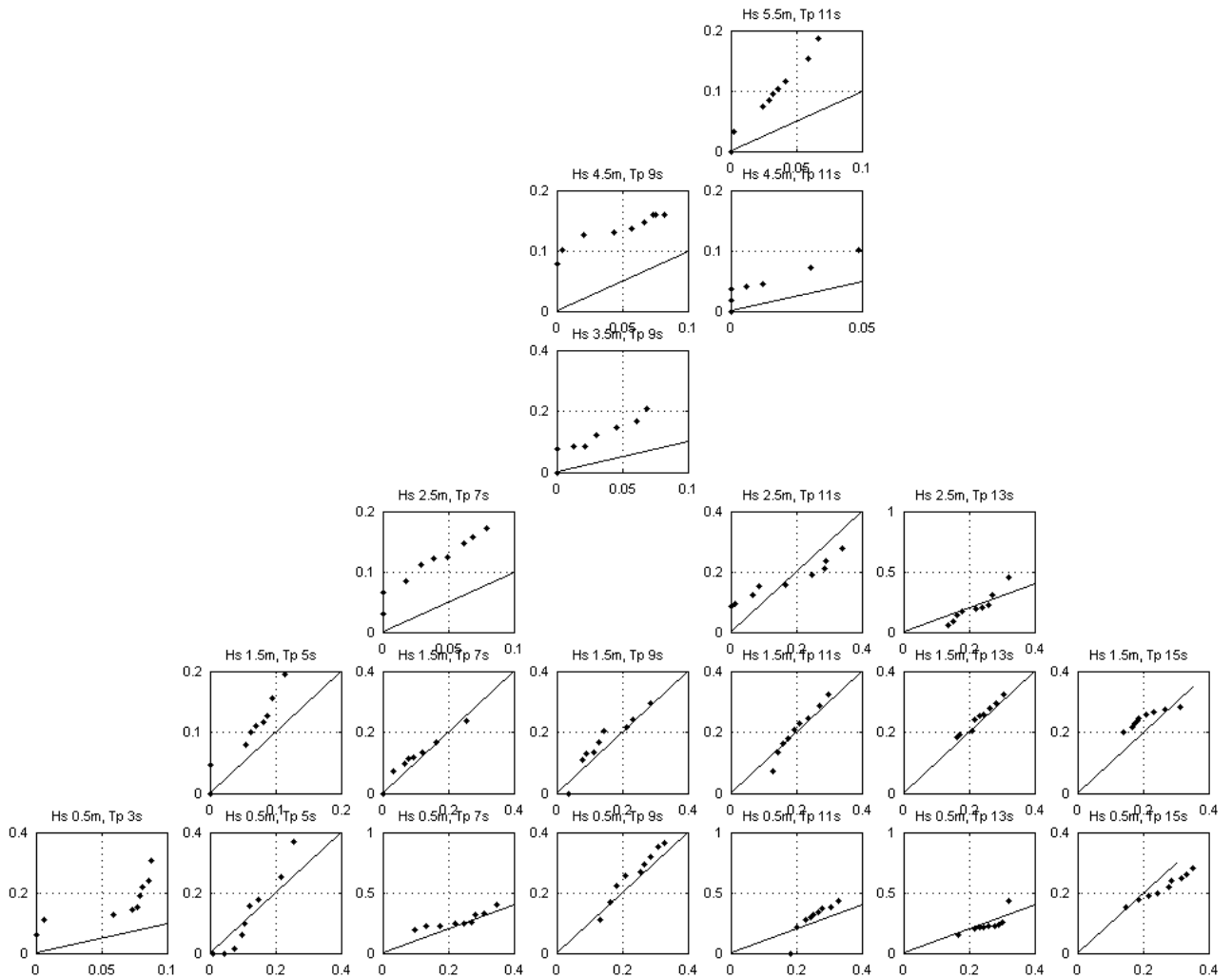


Figure 31 QQ plots for West of Shetland σ_b data (y-axis Seawatch, x-axis AES40)